

X-Ray Tomography Crystal Characterization: Automatic 3D Segmentation

Gautier Hypolite¹, Jérôme Vicente², and Philippe Moulin^{1,*}

¹Equipe Procédés Membranaires (EPM), Aix Marseille Univ., CNRS, Centrale Marseille, (M2P2 UMR 7340), Equipe Procédés Membranaires (EPM), Europôle de l'Arbois, BP80, Pavillon Laennec, Hall C, France

²Aix Marseille Univ., Institut Universitaire des Systèmes Thermiques Industriels (IUSTI-CNRS-UMR 6595), Technopôle de Château-Gombert, 5 rue Enrico Fermi, 13453 Marseille cedex 13, France

*Corresponding author: Philippe Moulin, E-mail: philippe.moulin@univ-amu.fr

Abstract

Understanding the structural parameters of crystals during crystal growth is essential for the pharmaceutical and chemical industries. This study proposes a new method for 3D images of crystals obtained with micro X-ray computed tomography. This method aims to improve the crystal segmentation compared to the watershed methods. It is based on plane recognition at the surface of the crystals. The obtained segmentation is evaluated on a synthetic image and by considering the recognized particle number and convexity. The algorithm applied to three samples (potassium alum, chromium alum, and copper sulfate) reduced oversegmentation by 87% compared to watershed based on ultimate erosion while keeping the convexity of the recognized particle.

Key words: crystallisation, Segmentation, surface recognition, X-ray tomography

Introduction

Understanding the structural parameters of crystals during growth is essential for the pharmaceutical and chemical industries. The crystal growth process determines properties of the final compound, such as its stability, facies, size distribution, and the polymorphism of crystals. In the pharmaceutical industry, crystals' shape can also affect the solubility, compatibility, and flow ability of bulk powders (Wang et al., 2008). All of these facts can impact product uniformity, dissolution, or bioavailability and therefore impact the safety and efficacy of the drugs (Turner et al., 2020). X-ray computed tomography (XCT) is a nondestructive imaging technique that allows the reconstruction of a sample in three dimensions, rotating through 360°, from radiographic projections (Thiery, 2015). The X-rays passing through the sample are attenuated (Kramers, 1923) and impregnate the detector to form an X-ray projection. These projections are recorded for a complete rotation. The greyscale X-ray image obtained at the detector is then recorded. Based on all these projections, a back-projection algorithm is used to provide volume density information (3D reconstruction) (Flannery et al., 1987), where the grey levels of the reconstructed image reflect a local density. We can then access the differences in composition and the presence of heterogeneities (pores, inclusions, etc.) within the sample. XCT has been used to study packing structures and determine topological quantities (size, distribution, contact numbers, contact angle distributions, and even contact surfaces) (Reimann et al., 2017). In the pharmaceutical industry, XCT has been used for the study of crystal powder, for example, to characterize the crystal powder microstructure (Gajjar et al., 2020) or to measure the particle packing of pharmaceutical design (Turner et al., 2020). In these studies

(Gajjar et al., 2020; Turner et al., 2020), XCT images are analyzed using a conventional watershed particle segmentation algorithm (Meyer & Beucher, 1990; Vincent & Soille, 1991). These analyses allow the volume, shape, and size distribution of particles in the crystal powder to be described. Nevertheless, specific image analysis methods must be (i) developed to study crystals to increase the accuracy of particle detection and (ii) be specifically relevant to the analysis of crystals. In particular, an accurate segmentation technique must be applied for particle recognition (Munch et al., 2006) and enhanced by considering specific morphological information of the crystals. Classic watershed segmentation methods (Meyer & Beucher, 1990; Vincent & Soille, 1991) that use distance map local minima as markers generally lead to oversegmentation (supernumerary detection of particles). A marker selection step reduces the number of segmented objects but requires the use of parameters based on the admissible objects' minimum sizes. These techniques may fail to identify oblong objects with several local minima (or even continuous lines of local minima for cylindrical objects or a plane of local minima for flat objects). Moreover, crystals can present structures for which the distance map local minima, obtained by calculating the ultimate erosion, can be multiple for the same object, leading to oversegmentation. Moreover, even if crystals are theoretically convex, in reality, 3D XCT crystal objects contain slight concavity due to surface irregularities or to inclusions. The concavities can create, locally, small objects within the same crystal. Finally, applying a conventional watershed algorithm to crystal images would result in excessive particle segmentation. Several approaches have been developed to avoid the oversegmentation due to the use of the watershed: (i) Beucher (1994) suggests computing a watershed transform on an image derived from the original image. The

method relies on the fact that the gradient values are lower inside a region than between two regions. This method allows the reduction of oversegmentation from classical watershed with no free parameters. (ii) Another approach is proposed by Faessel & Jeulin (2010). This is based on the calculation of the probability density function (*pdf*) of the points of belonging to the contours of the watershed. The segmentation is obtained by applying a flat zone labelling on the *pdf*. Here too, the method reduces oversegmentation without having to supply markers. The segmentation is obtained with no parameter. (iii) Munch et al. (2006) present a computational procedure to segment particles from 3D volumes (in their case, acquired with focused ion beam–nanotomography). The method is an enhanced watershed approach for 3D particle segmentation. In this method, the oversegmentation is controlled through a free parameter (*k*-value) for accurate object recognition. The method is developed to be specifically valuable for analyzing granular textures. It is based on a suitable segmentation technique associated with correct particle recognition. This modified watershed technique tolerates some concavities on the particle surfaces. As we are looking to analyze crystals, the segmentation methodology can be enhanced by considering crystal properties. Crystals are solid in which the constituents are regularly combined, and their surfaces are mostly planar. Watershed segmentation can be improved using these properties.

The aim of this work was to develop a methodology to improve crystal analysis by XCT. Crystal automatic segmentation enables the quantification of the different crystal typologies and fine characterization of their size distribution. The method is based on watershed segmentation and plane recognition. We propose a novel algorithm: to individualize crystals from 3D tomographic images and to efficiently separate aggregated crystals. This image analysis method adapted to crystal specificity should be sufficiently robust to study crystal processing and formation. The methodology is based on crystal face identification and classic 3D volume segmentation of aggregates. The final crystal segmentation is then evaluated by analyzing the distribution of crystal shapes. We will study the crystals formed by three different chemical species formed under different crystallization conditions. Potassium alum [potassium aluminum sulfate dodecahydrate— $\text{K}(\text{SO}_2)_2 12(\text{H}_2\text{O})$, $\text{Al}(\text{SO}_2)_2 12(\text{H}_2\text{O})$], chromium alum [potassium chromium sulfate dodecahydrate— $\text{Cr}(\text{SO}_2)_2 12(\text{H}_2\text{O})$, $\text{Al}(\text{SO}_2)_2 12(\text{H}_2\text{O})$], and copper sulfate ($\text{CuSO}_4 5\text{H}_2\text{O}$) are chosen for these experiments as they are readily available and present different crystal shapes.

Materials and Methods

Chemicals and Preparation

Three chemical species were chosen for the experiment, and saturated solutions were made with them: (i) potassium alum (double sulfate of potassium and aluminum dodecahydrate, 99.5% purity, Fisher Scientific) at 60°C, (ii) chromium alum (double sulfate of potassium and chromium dodecahydrate, 99% purity, Fisher Scientific) at 55°C, and (iii) copper sulfate pentahydrate ($\text{CuSO}_4 5\text{H}_2\text{O}$) at 60°C (99% purity, Fisher Scientific). Distilled water was used for solution preparation. The solutions were placed in a test tube (Fig. 1a) in which three cotton yarns were installed for crystals to grow on them and to prevent crystals from falling to the bottom of the tube. Figure 1a presents a schema of the test tubes

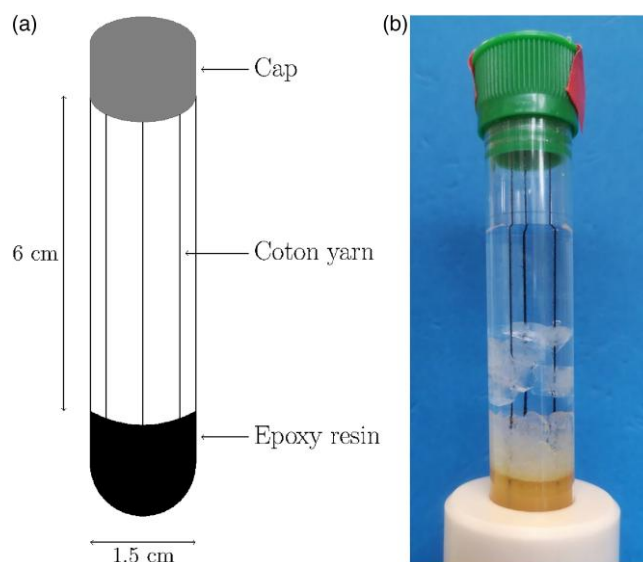


Fig. 1. Test tube used for XCT: (a) diagram of the test tube with the three cotton yarn; (b) photo of a crystallized potassium alum sample.

that were used for the experiment. The solution was cooled down to room temperature to let the alum recrystallize. An example of crystals is presented in Figure 1b.

X-Ray Computed Tomography

Micro-CT scans were performed with an EasyTomXL150 “Mechanic Ultra” microtomograph (RX Solutions, France) to determine the crystal structure in the test tube. An X-ray attenuation higher than the liquid region characterizes the crystals due to its structure. Scans were performed at 103 and 172 mA. The number of radiographic projections was 1120, which corresponds to an angle step between projections of 0.32°. To increase the signal to noise ratio, each tomographic projection was obtained by means of 3 successive images for the same angular position. The total scan time was approximately 30 min. The voxel size achieved under these conditions was 32 μm ($x = y = z$), and the region of interest (ROI) was 1437 \times 1392 \times 1437 mm ($x \times y \times z$). The obtained 3D volume consists of voxels characterized by their greyscale value (GSV) ranging from 0 to 65,535 for a 16-bit image, depending on the X-ray attenuation of the sample. An increase in the GSV corresponds to higher X-ray attenuation. The 16-bit images are converted to 8-bit images characterized by a GSV ranging from 0 to 256. Figure 2a shows an example of a greyscale image obtained with XCT of a potassium alum sample. The figure is a cut orthogonal to the tube axes. Afterward, the greyscale images were converted to binary images (Fig. 2b) representing the crystals. The conversion was performed by applying a noise filtering process, followed by a threshold operation. Noise filtering was carried out by applying a nonlocal mean denoising filter with a sigma value of 15 and a smoothing factor of 1. The solid phase (crystals) was separated from the liquid phase by thresholding the greyscale image. The threshold value used for the binarization was obtained using the Shanbhag method (Shanbhag, 1994). The black part of the image is the solid phase (crystals), and the white part is the liquid phase. The method provides a binary 3D image made of voxel. The solid surface is meshed using the marching cubes algorithm (Lorenson & Cline, 1987) with the same threshold

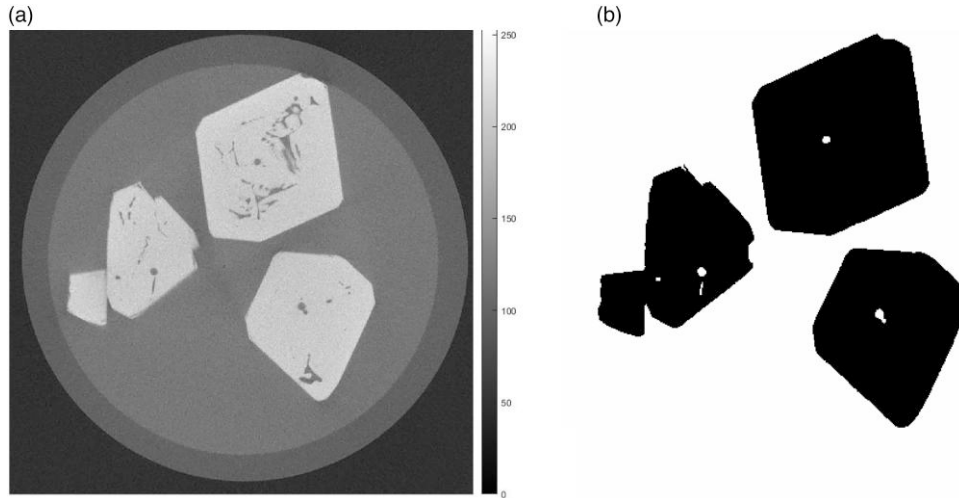


Fig. 2. Example of a cut in the 3D images obtained with XCT: **(a)** Original gray image and **(b)** binary image.

value that was used to separate the solid and liquid phases. The marching cubes algorithm scans the 3D image; for each group of 8 voxels defining a cube, the polygons of the mesh to be created (if there is a polygon to create) are determined.

The novelty of this study is to propose a new method to analyze the obtained 3D binary images. The general principle of the method we developed is to apply the Münch segmentation method and merge the obtained particles that share a face (or several faces). Indeed, if two particles share the same face, they belong to the same crystal. It is then necessary to identify the crystal faces (i.e., flat surface) in the 3D images. Therefore, we will present the following: (i) the particle identification with the Münch segmentation method, (ii) the face recognition algorithm, (iii) crystal segmentation that consists of merging particles that share a face, and (iv) evaluation criteria of the obtained results which describe particle convexity.

Particle Identification

On one hand, the initial segmentation (before merging particles that share a face) must give at least one particle per crystal (i.e., no undersegmentation) to ensure that each crystal can be recognized separately after the merge. On the other hand, the method should not produce too much oversegmentation or the merging step will not be able to correctly reconstruct the crystals. The Munch et al. (2006) method was preferred to the Beucher (1994) method as it is more suitable for granular texture analysis, especially as the crystals have a similar greyscale value. Therefore, touching crystals will be merged with the Beucher method and this will result in undersegmentation. The Münch method was also preferred to the Faessel & Jeulin (2010) method as it allows shorter computational time. In addition, the Münch method has a free parameter, the k -value, which allows the control of the initial segmentation. The interest of such a control here is to ensure that there is no undersegmentation and also to prevent too much oversegmentation. In addition, the Münch et al. method allows for concavities on the crystals' surfaces. The method consists of four steps to identify the individual particles: (i) a distance map $D(x, y, z)$ is obtained using a Euclidean distance transform, (ii) the image mask is eroded iteratively by increasing the eroding distance d_j (j denotes the iteration number), and (iii) at each iteration, a particle p_i (i denotes the particle index)

is divided in two or more particles p_{i1} and p_{i2} if some fragmentation constraints are met [Eq. (1)],

$$d_j < k \cdot r_{p_{i1}} \text{ and } d_j < k \cdot r_{p_{i2}}, \quad (1)$$

where r_{p_i} is the maximum distance from the interior of the particle p_i to the surface boundaries. k is a control parameter between 0 and 1 that can be set for proper fragmentation regulation, thereby allowing an appropriate segmentation to be achieved. (iv) Eroded particles are reconstructed by dilating them back to the original boundaries. The number of segmentations increases with the k value, and the limit value of $k = 1$ corresponds to the watershed segmentation using ultimate erosion calculation (this limit will be named watershed ultimate in this paper). An example of the obtained segmented image is presented in Figure 3 for different values of the k parameter.

Face and Crystal Identification

Planar surface recognition in 3D images has been widely studied to identify planes in point clouds (Hulik et al., 2014). Three main methods have been studied for 3D point clouds: region growing (Poppinga et al., 2008), Hough transform (Hough, 1962), and random sample consensus (RANSAC) (Fischler & Bolles, 1987). Hulik et al. (2014) present an analysis of the main methods used in the literature for plane recognition: (i) The Hough transform algorithm (Hough, 1962) allows arbitrary parameterized shapes (lines, circle, plane, etc.) to be recognized in point cloud but is more time consuming than the other method. (ii) RANSAC (Fischler & Bolles, 1987) is a nondeterministic algorithm and thus allows model fitting without trying all possibilities. The main concept is to randomly select a minimal subset to define the model and to check which elements of the entire dataset are consistent with the model. For plane detection (Schnabel et al., 2007), random planes (passing through three randomly selected points) are evaluated. A score function is used to determine how good the model fits the remaining points. The score takes into account the number of points close enough to the plane. A plane with the best score is taken as a winner. (iii) Region growing algorithms start with a seed region and grow it to its neighborhood when the neighbors satisfy some conditions.

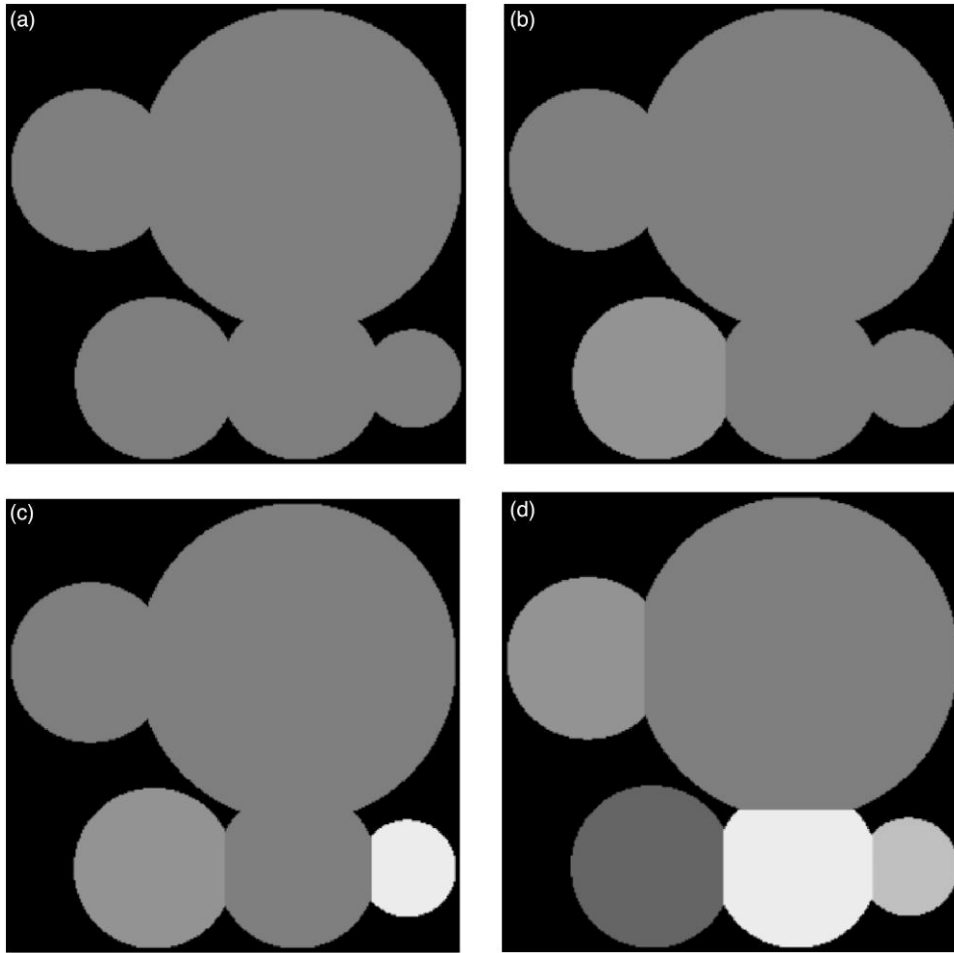


Fig. 3. Segmentation of the object made of a combined sphere according to the value of parameter k from Munch et al. (Munch et al., 2006) method [inspired from (Munch et al., 2006)]: (a) $k=0.4$, (b) $k=0.5$, (c) $k=0.7$, and (d) $k=0.8$.

Region growing algorithms are rapid when there are many planes to extract but need an organized 3D point cloud in which neighbors of every point are known. Here, the solid surface is meshed [with the marching cubes algorithm (Lorenson & Cline, 1987)]; therefore, plane detection can be performed on mesh cells rather than on point cloud. In this way, a modified region growing algorithm can be applied as neighbors of each cell are known. Plane identification is applied to the surface mesh of the solid phase. The mesh consists of a set of triangles. The nodes, normal of triangles, and each triangle's neighbors are known (for each triangle, we compute the list of triangles that share almost one node with the considered triangle). A first step of the algorithm consists of computing the triangle's normals. The values of the normals are smoothed by taking into account the normals of adjacent triangles. The objective is to denoise the surfaces obtained by the marching cubes methodology. Indeed, the mesh can present irregularities on the flat surfaces. For that, node normals are computed as the average of the adjacent triangle normals. The face normals are recomputed as the average of the normal of the nodes that make up the face. Then, planes are identified and labeled using region growing techniques. Starting from a first triangle of the mesh, the face is constructed by iteratively adding neighboring triangles, checking a coplanarity criterion, to the face. Each time a triangle is added to the face being labeled, the average normal of this face is updated. The normal of the

face is used in the coplanarity test, which allows a new triangle to be added if the angular deviation between this triangle and the face is below a given threshold. Once the propagation is stopped, a new unlabeled triangle is used to constitute a new face. Once all the triangles are labeled, a face fusion step is used to group the adjacent faces through a new coplanarity criterion. The faces are previously sorted according to their surface area. The fusion of the faces begins with the faces of the larger surface area, supposed to represent the facets of the crystals. The new coplanarity criterion is based on two conditions: the slight angular deviation between the two adjacent faces and the small distance of the center of gravity of the face to be merged with the plane of the face. Once the faces have been identified, each labeled node is associated with the nearest crystal voxel. Thus, labeling the faces allows a map of voxels whose labels correspond to the faces to be obtained. In the last phase, too small faces are eliminated. The face detection algorithm is dependent on the starting point. Indeed, the first point determines the first normal. For this reason, this normal is recalculated during propagation. That reduces the dependence on the starting point. The dependence on the starting point is also smoothed when in a second step; the surfaces are merged based on the coplanarity criterion. For this merging step, the planes are classified by size, which also minimizes the impact of the starting point. Finally, only the largest surfaces are kept (using a minimal size criterion). The

largest surfaces resulting from merging different surfaces are not too dependent on the starting point, unlike small surfaces, potentially resulting from a first aberrant normal. [Figure 4](#) shows an example of the result of the face recognition algorithm: the algorithm has been applied to a 3D computer synthetic image. The 3D image is presented in [Figure 4a](#); it is made of 11 unarranged octahedra, and the number of planes to detect is 88 (eight per octahedra). The algorithm gives a good identification of the crystals' faces: exactly 88 faces are recognized ([Fig. 4](#)). As shown in [Figure 4b](#), the algorithm enables the crystal surface to be constructed. However, the methods are not sufficient to construct the crystals' 3D models. Indeed, faces do not entirely close the crystals: contact faces between two crystals are not recognizable.

Crystal Segmentation

The 3D crystal models are constructed by merging particles from the Münch et al. method in contact with the same plane. The method consists first in identifying for each face the particles in contact. The volumes in contact with the same face are merged, and the interconnection graph that allows for the identification of the other faces in contact with these objects is then updated. The voxels of faces are necessarily voxels of crystal particles, which facilitate the search for particles in contact with the faces. First, the method is tested on a synthetic image. The same image as for the plane recognition validation is used. Then, the method is applied to a real sample and evaluated with two criteria: the number of recognized particles and the convexity of the particles. The number of recognized particles is used to evaluate the oversegmentation (the objective is to not recognize too many particles). The convexity is used to evaluate the undersegmentation (too few particles). Unlike a particle describing a single crystal, a unique particle that describes a cluster of crystals will not be convex. Therefore, a good segmentation should give the minimum number of particles while keeping the recognized particle convex.

Convexity of the Recognized Particle

The convexity of recognized particles is used as a criterion to evaluate the method. We defined the convexity rate of the particle as the ratio of the particle's convex hull volume to the particle's volume. The particle's convex hull is the smallest convex envelope that contains the particle. Then, the convexity rate describes the difference between the recognized particle and an ideal particle. The convexity rate is between 0 and 1, and the closer the value is to one, the more convex is the particle. The convex hull of each particle is determined to compute the convexity rate. The convex hull is computed using the quick hull algorithm ([Barber et al., 1996](#)). The implementation of this algorithm is done using CGAL (The Computational Geometry Algorithms Library) ([Alliez & Fabri, 2016](#)). The quick hull algorithm gives a mesh of the convex hull. The volume of the convex hull is computed by determining if the 3D image voxels are inside or outside of the hull.

Shape of the Recognized Particles

The equivalent diameter (D_e) is used to describe the particle size. It is defined as the diameter of the sphere having the

same volume as the particle [Eq. (2)],

$$D_e = 2 \cdot \left(\frac{3}{4} \cdot \frac{V_p}{\pi} \right)^{\frac{1}{3}}, \quad (2)$$

with V_p being the particle volume.

The equivalent diameter gives information about particle sizes but does not describe the particles' shape. Therefore, the lengths of the covariance ellipsoid axes are computed to evaluate the particles' shape. These lengths correspond to the square root of the covariance matrix eigenvalue. The ratio of the two minor axes on the major axis length named (R_a and R_b) is used to describe the shapes. [Gajjar et al. \(2020\)](#) suggest using another metric to describe the shape: the particles' sphericity. Sphericity (S) describes the proximity between an object's shape and a sphere. It is defined as the ratio between the surface of a sphere of the same volume as the object and the surface of the object (A_p) [Eq. (3)],

$$S = \frac{\pi^{\frac{1}{3}}(6V_p)^{\frac{2}{3}}}{A_p}. \quad (3)$$

Results and Discussion

Evaluation of the Crystal Segmentation

First, the algorithm is tested on a synthetic image; the image of [Figure 4](#) is used again. It consists of a stack of 11 octahedrons. The problem related to the use of a computer-generated image is that the image is completely filled (with no inclusions), and surfaces are perfect (perfectly flat with no concavities), though we note that it is possible for computer-generated images to exhibit grains with rough or concave boundaries ([Figliuzzi, 2019](#)). The Münch et al. algorithm applied to this image leads directly to the correct segmentation. Therefore, a small number of concavities are added inside the volume. Twenty-two of the 2,240,380 solid voxels are changed to liquid voxels to form individual cavities. These cavities in the solid phase can be observed in the real images. They correspond to liquid inclusions, to the cotton yarn, or due to weak contrast voxels. The cavities additions lead to oversegmentation with the method of Münch et al. Indeed, their algorithm recognized 59 particles, while 11 crystals are on the image. The result of the Münch segmentation is presented in [Figure 5a](#) (3D image) and [Figure 5b](#) (cross-section view). The algorithm developed for this study (named crystal recognition algorithm) has been applied on the same image. The result is presented in [Figure 5c](#) (3D image) and [Figure 5d](#) (cross-section view). The crystal recognition algorithm recognized 11 particles. This number corresponds to the number of crystals to identify. Validation of segmentation is a difficult task for which the human eye is an effective tool. [Figure 5](#) images clearly show the improvement obtained with the crystal recognition algorithm. The oversegmentation from Münch et al. can be seen in [Figures 5a and 5b](#). In contrast, the particles identified by the crystal segmentation algorithm, shown in [Figures 5c and 5d](#), fit well with the crystals. Therefore, the recognition ability of the crystal recognition algorithm is validated on the computer-generated image.

XCT was performed on three samples of crystallized solution. The first sample was potassium alum, the second, chromium alum, and the third, copper sulfate. Particle identification was performed with three algorithms: watershed

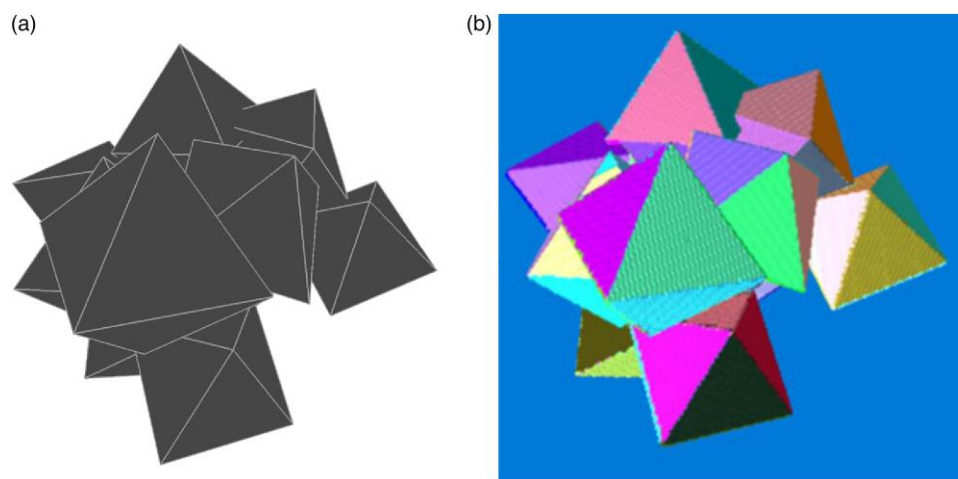


Fig. 4. 3D image of a pile of 11 unarranged octahedra. **(a)** 3D mesh of the image: it contains 88 faces. **(b)** Plane identified with the plane recognition algorithm. Eighty-eight planes are recognized in the 3D image.

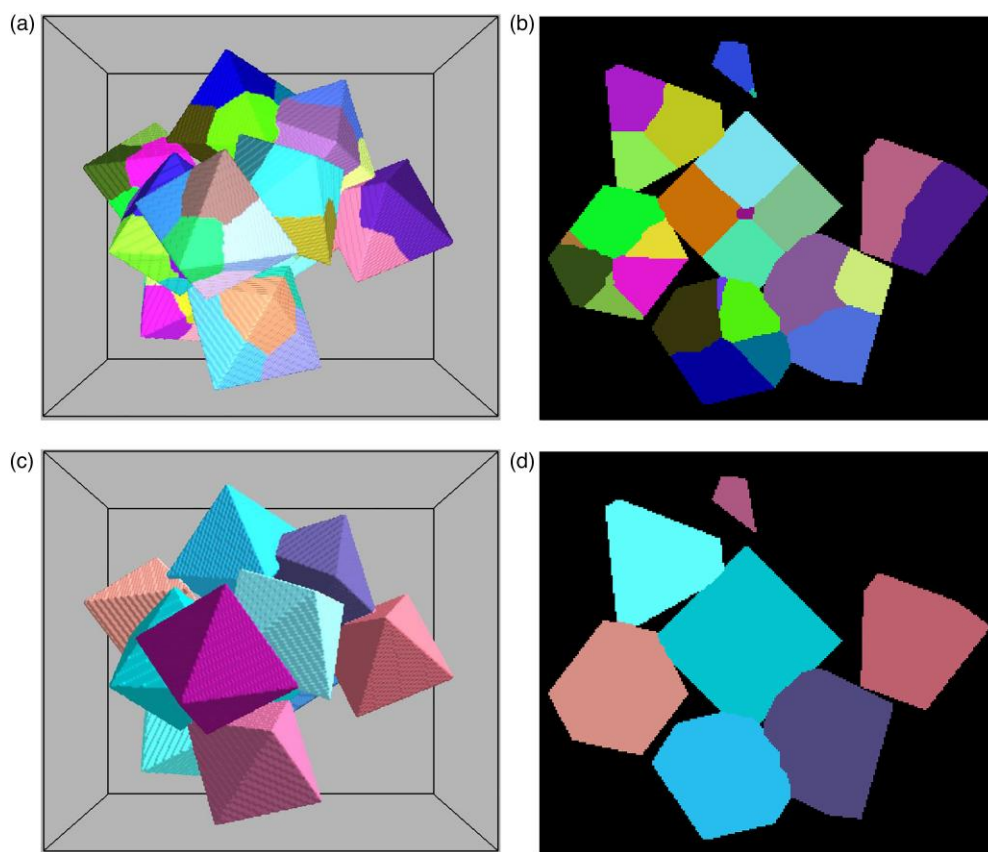


Fig. 5. Particle recognition on a 3D synthetic image (pile of 11 unarranged octahedra). Each color represents a recognized particle. Münch et al. algorithm result: **(a)** 3D visualization and **(b)** view of a cut plane. Crystal recognition algorithm result: **(c)** 3D visualization and **(d)** view of a cut plane.

ultimate algorithm, the Münch et al. algorithm, and the crystal recognition algorithm. Figure 6 presents the number of recognized particles and the mean particle convexity obtained with the three algorithms applied to the potassium alum sample according to the value of the k parameter. The right axis, describing the number of particles, has a logarithmic scale. Increasing the value of k leads to an increase in the number of recognized particles while reducing the convexity ratio. When the k value approaches 1, the number of particles

increases very quickly, corresponding to oversegmentation. A proper segmentation algorithm should give the minimum number of particles with the highest convexity ratio. The value of k equal to 0.98 was selected because it allows for an important reduction of the number of particles compared to the maximum value of 1, and it corresponds to the convexity ratio maximum. Results are similar for the two other samples; therefore, the k value of 0.98 has also been used on these samples. For a small k value (under 0.9), the crystal segmentation

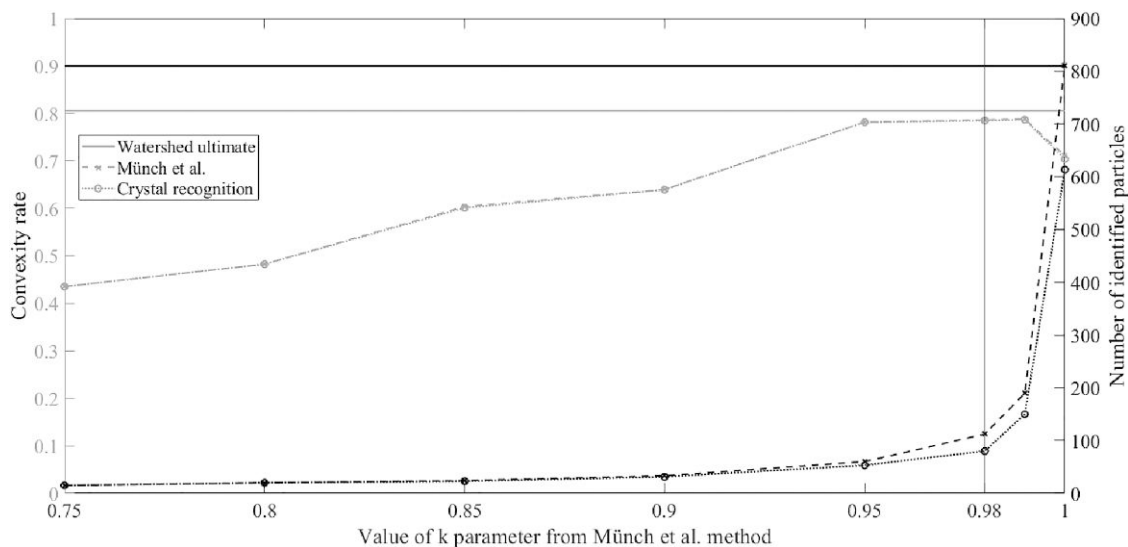


Fig. 6. Result of recognition particle algorithms applied to the potassium alum sample. Mean value of the convexity ratio according to the k parameter (left axis) and number of recognized particle according to the k parameter (right axis).

does not merge any particle as the recognized particles from Münch et al. are too big and already correspond to at least one crystal. Therefore, for these k values, the results of the Münch et al. method and crystal segmentation algorithm are the same. For the optimal k value of 0.98, the number of particles recognized with the crystal recognition algorithm is approximately 25% lower than the number recognized with the Münch et al. method. However, the convexity rate obtained with the crystal recognition algorithm remains really close to the value obtained with the Münch et al. method independently of the k value. Finally, the crystal recognition algorithm allows the number of recognized particles to be significantly reduced, and the conservation of the convexity ratio allows us to conclude that the algorithm does not merge different crystals, i.e., the particles are merged in the same crystals, reducing oversegmentation.

Figure 7 shows the segmentation obtained with the crystal segmentation algorithm applied to the three samples. Figure 7 shows the front view of 3D images of potassium and chromium alum. For copper sulfate, the top view is presented, as the large number of crystals mask the segmented crystals. The crystal structure can be identified in the 3D image: potassium and chromium alum crystallize in the shape of truncated octahedrons, which is the typical form in which these species crystallize in, and copper sulfate forms elongated crystals. Potassium and chromium form a small number of big crystals while copper sulfate forms a large number of smaller crystals which explains the choice of these compounds chosen to test the developed algorithm.

The segmentation presented in Figure 8 appears to describe crystals correctly. The convexity ratio distribution is used to quantify the performance of the method. It has been computed on the particles obtained with the Münch et al. method and the crystal recognition algorithm applied to the three samples. The distribution of convexity is presented in Figure 8. Particles obtained on the same sample with the Münch et al. algorithm and the crystal recognition algorithm have a very similar convexity distribution. The maximum absolute difference between the convexity obtained with the two algorithms on a same sample is 2.5% although it is mostly below 1% except

for two values. At least 50% of the particles have a convexity rate higher than 0.9, and 90% of them have a convexity rate higher than 0.7. Conservation of convexity between the two algorithms means that the new algorithm does not produce more undersegmentation (too few particles). Therefore, the reduction of particle number while keeping the convexity reflects a better description of the crystals. Finally, the high convexity of recognized particles and the similarity between the convexity of particles from the Münch et al. method and the method presented in this paper allow us to validate the merging method that has been developed.

Crystal Size and Structures

The purpose of the crystal segmentation algorithm is to separate individual crystals to compute metrics on them. In particular, the size and shape of crystals are important regarding their physical properties. Based on the crystal segmentation, the particle diameter distributions were calculated and expressed in terms of cumulative volume (Q3). For practical applications, it can be easier to use the characteristic equivalent diameter D_n than the complete distributions: such a metric corresponds to the cell diameter for which $n\%$ of the volume distribution has smaller cell sizes and $(100-n)\%$ has larger cell sizes (Petlitchkaia et al., 2021). The cumulative value Q3 for the potassium alum sample is presented in Figure 9. Watershed ultimate led to the smallest particle size, due to oversegmentation: D10, D50, and D90 values are half of those obtained with the crystal segmentation algorithm. The Münch et al. method reduces oversegmentation; therefore, crystal size is increased compared to the watershed method. The crystal segmentation algorithm gives a bigger particle size than other algorithms, especially as the number of small particles is reduced compared to the Münch method.

Table 1 summarizes the shape, the size, and the structure metrics that have been computed on the recognized crystals. The number of crystals recognized by the crystal recognition algorithm is significantly lower than the number obtained with the Münch et al. method: the number of recognized particles is reduced by 29, 39, and 12% for potassium alum,

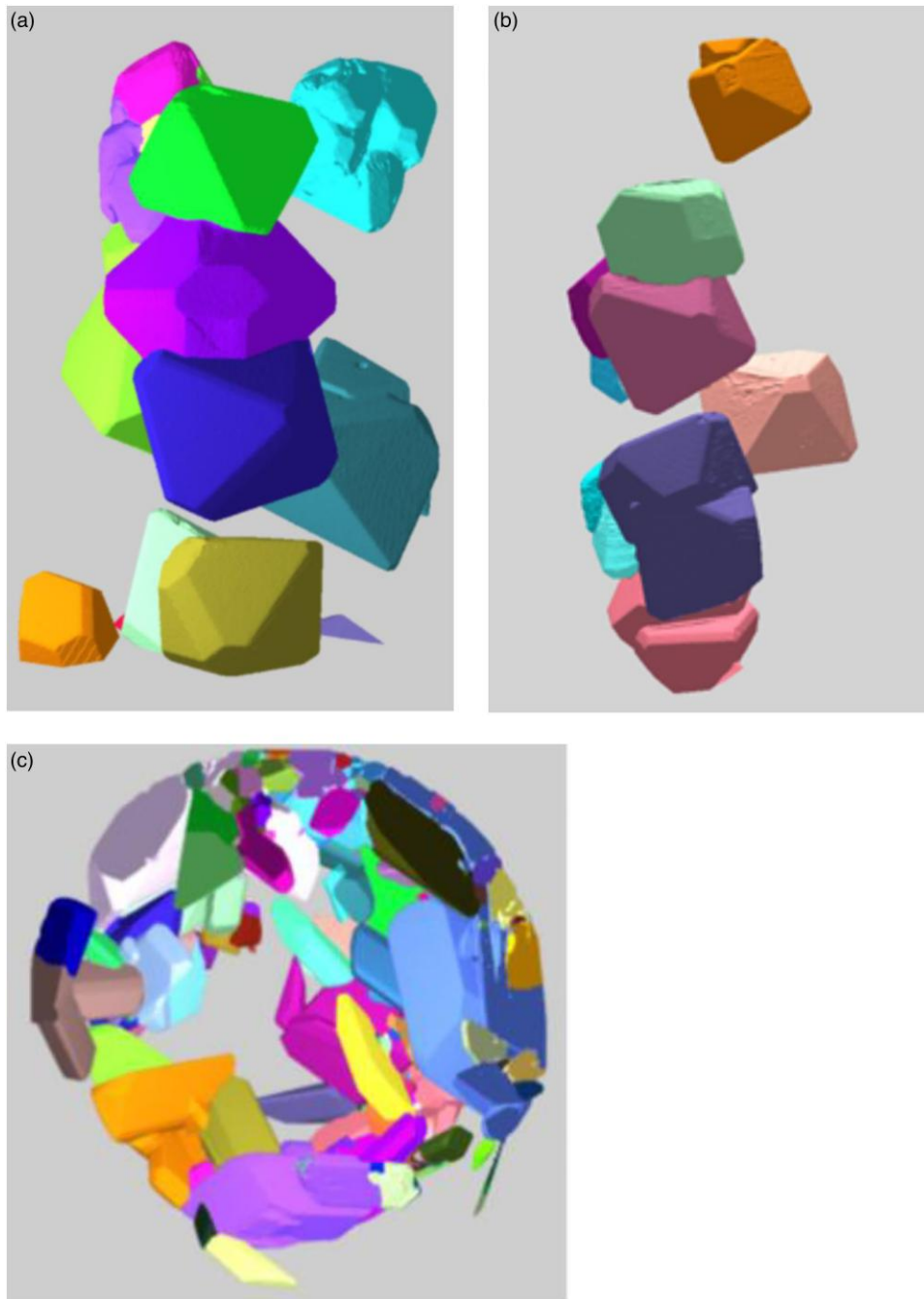


Fig. 7. 3D images presenting the crystal segmentation applied on XCT images: **(a)** potassium alum—front view, **(b)** chromium alum—front view, and **(c)** copper sulfate—top view.

chromium alum, and copper sulfate, respectively. Therefore, crystals recognized with the crystal recognition algorithm are bigger than the ones recognized by the Münch et al. method. In the same way, as seen for the potassium alum sample in Figure 9, the D10 value increases significantly (around 20%) while D50 and D90 values remain almost unchanged. This indicates that the algorithm mainly merges the small particles to big particles.

Potassium alum and chromium alum have similar size distributions ($D_{50} \approx 4.4$ mm). They also have a similar shape which is indicated by a similar sphericity value ($S \approx 0.5$) and similar equivalent ellipse shape ($R_a \approx 0.6$ and $R_b \approx 0.5$). Indeed, there

are two similar components that have been prepared similarly. Copper sulfate crystals are smaller than potassium and chromium alum crystals ($D_{50} \approx 1.6$ mm). Copper sulfate crystals form elongated crystals which are seen in Figure 7c. This shape corresponds to a small sphericity value ($S \approx 0.36$) and elongated equivalent ellipse ($R_a \ll 1$ and $R_b \gg 1$). Crystal recognition algorithm allows the shape description to be improved, especially for long crystals such as copper sulfate crystals. Indeed, the sphericity value is reduced for the copper sulfate, especially that the ratio R_a and R_b is reduced by a factor of 4. This is explained by the fact that the Münch et al. algorithm tends to fragment long crystals.

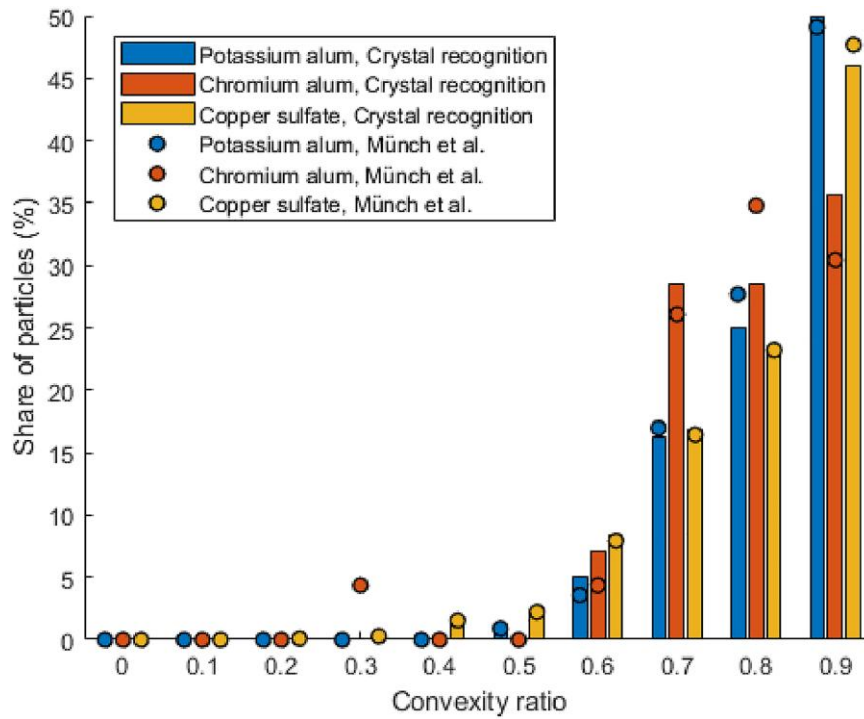


Fig. 8. Distribution of particle convexity ratio obtained with crystal recognition algorithm (bars) and Münch et al. method (circles) applied on the three samples.

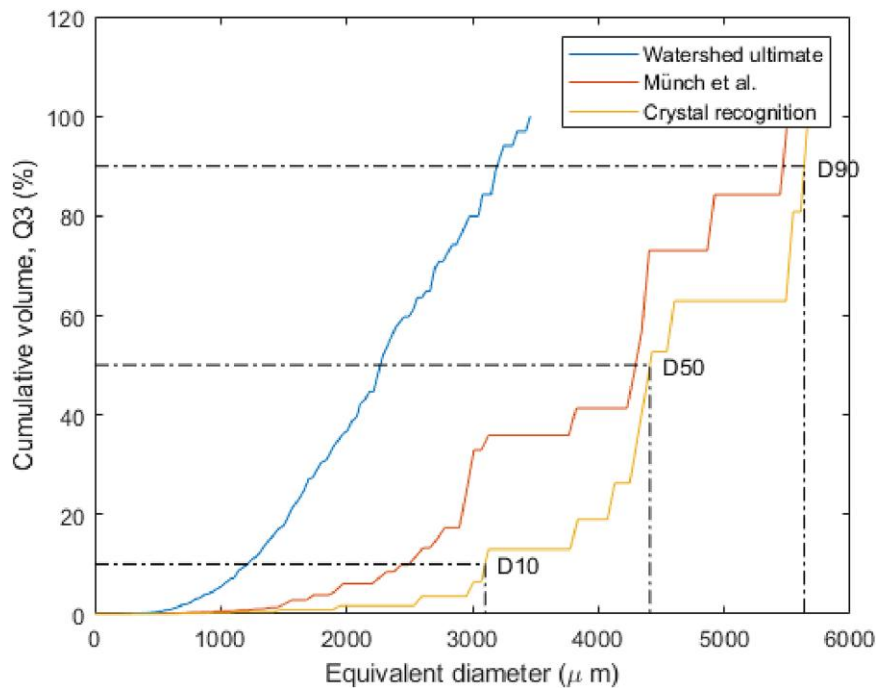


Fig. 9. Distribution of the recognized particle-representative diameter express in terms of cumulative volume Q3 for the potassium alum sample.

Conclusion

In this study, we developed a new method specific to crystal recognition in 3D images obtained with XCT. The method is based on a particle segmentation algorithm coupled with a plane recognition algorithm. Particles that share the same face are part of the same crystal. This new method has been

validated on a synthetic image (crystals + defects) and compared to other recognition methods. It shows a good segmentation of crystals: all crystals on the image are recognized and there are no additional particles. The crystal recognition algorithm shows a better result with fewer recognized particles than existing methods. The number

Table 1. Shape and Structure Metrics From Segmentation Algorithms Applied to Potassium Alum, Chromium Alum, and Copper Sulfate Samples.

Sample Algorithm	Potassium Alum		Chromium Alum		Copper Sulfate	
	Münch	Crystal Segmentation	Münch	Crystal Segmentation	Münch	Crystal Segmentation
Number of particles	112	80	23	14	60	53
D10 (mm)	2.49	3.10	2.71	3.31	0.69	0.55
D50 (mm)	4.29	4.41	3.76	4.44	1.50	1.58
D90 (mm)	5.47	5.63	5.45	5.43	2.98	2.77
Mean sphericity	0.49	0.48	0.52	0.51	0.41	0.36
R_a	0.71	0.60	0.75	0.63	0.62	0.14
R_b	0.51	0.43	0.56	0.54	0.42	0.10
Mean convexity	0.79	0.79	0.80	0.79	0.69	0.69

of recognized particles is 8 times lower than that with a watershed on ultimate erosion and 30% lower than that with the Münch et al. method. The lower number of particles means that the method leads to less oversegmentation. The segmentation was validated with convexity criteria on recognized particles: the convexity is similar to the one obtained with the existing algorithms. The identification of individual crystals enables the shape and structure of the crystals to be determined. The metrics on crystal shape were improved using the crystal segmentation algorithm compared to the Münch et al. method, especially in the identification long crystals. Here, two types of alum and copper sulfate were analyzed: potassium alum and chromium alum have a similar size and shape (truncated octahedron), whereas copper sulfate crystals are bigger and have an elongated shape.

Availability of Data and Materials

The authors have declared that no datasets apply for this piece.

Financial Support

The project leading to this publication has received funding from the IMI (Institut Mécanique et Ingénierie, Aix Marseille University).

Conflict of Interest

The authors declare that they have no competing interest.

References

Alliez P, & Fabri A (2016). CGAL: The computational geometry algorithms library. In *ACM SIGGRAPH 2016 Courses*, pp. 1–8. New York: Association for Computing Machinery.

Barber CB, Dobkin DP & Huhdanpaa H (1996). The quickhull algorithm for convex hulls. *ACM Trans Math Software* 22(4), 469–483. <https://doi.org/10.1145/235815.235821> SMASH

Beucher S (1994). Watershed, hierarchical segmentation and waterfall algorithm. In *Mathematical Morphology and Its Applications to Image Processing*, vol. 2, Serra J & Soille P (Eds.), pp. 69–76. Dordrecht: Springer Netherlands

Faessel M & Jeulin D (2010). Segmentation of 3D microtomographic images of granular materials with the stochastic watershed: SEGMENTATION OF 3D IMAGES. *J Microsc* 239(1), 17–31. <https://doi.org/10.1111/j.1365-2818.2009.03349.x> SMASH

Figliuzzi B (2019). Eikonal-based models of random tessellations. *Image Anal Stereol* 38, 15–23. <https://doi.org/10.5566/ias.2061> SMASH

Fischler MA, & Bolles RC (1987). Perceptual organization and curve partitioning. In *Readings in Computer Vision*, pp. 210–215. Menlo Park, CA: Elsevier.

Flannery BP, Deckman HW, Roberge WG & D’Amico KL (1987). Three-dimensional X-ray microtomography. *Science* 237(4821), 1439–1444. <https://doi.org/10.1126/science.237.4821.1439> SMASH

Gajjar P, Styliari ID, Nguyen TTH & Murnane D (2020). 3D characterisation of dry powder inhaler formulations: Developing X-ray micro computed tomography approaches. *Eur J Pharm Biopharm* 151, 32–44. <https://doi.org/10.1016/j.ejpb.2020.02.013> SMASH

Hough PVC (1962). Method and means for recognizing complex patterns. Retrieved from <https://patents.google.com/patent/US3069654/en>

Hulik R, Spanel M, Smrz P & Materna Z (2014). Continuous plane detection in point-cloud data based on 3D Hough transform. *J Vis Commun Image Represent* 25(1), 86–97. <https://doi.org/10.1016/j.jvcir.2013.04.001> SMASH

Kramers HA (1923). XCIII. On the theory of X-ray absorption and of the continuous X-ray spectrum. *London, Edinburgh, Dublin Philos Mag J Sci* 46(275), 836–871. <https://doi.org/10.1080/14786442308565244> SMASH

Lorensen WE & Cline HE (1987). Marching cubes: A high resolution 3D surface construction algorithm. *ACM SIGGRAPH Comp Graph* 21(4), 163–169. <https://doi.org/10.1145/37402.37422> SMASH

Meyer F & Beucher S (1990). Morphological segmentation. *J Vis Commun Image Represent* 1(1), 21–46. [https://doi.org/10.1016/1047-3203\(90\)90014-M](https://doi.org/10.1016/1047-3203(90)90014-M) SMASH

Munch B, Gasser P, Holzer L & Flatt R (2006). FIB-nanotomography of particulate systems—Part II: Particle recognition and effect of boundary truncation. *J Am Ceram Soc* 89(8), 2586–2595. <https://doi.org/10.1111/j.1551-2916.2006.01121.x> SMASH

Petlitckaia S, Vincente J & Poulesquen A (2021). Characterization of a geopolymer foam by X-ray tomography. *Front Chem* 9, 754355. <https://doi.org/10.3389/fchem.2021.754355> SMASH

Poppinga J, Vaskevicius N, Birk A, & Pathak K (2008). Fast plane detection and polygonalization in noisy 3D range images. In *2008 IEEE/RSJ International Conference on Intelligent Robots and Systems, Nice*.3378–3383. New York City, USA: IEEE.

Reimann J, Vicente J, Brun E, Ferrero C, Gan Y & Rack A (2017). X-ray tomography investigations of mono-sized sphere packing structures in cylindrical containers. *Powder Technol* 318, 471–483. <https://doi.org/10.1016/j.powtec.2017.05.033> SMASH

Schnabel R, Wahl R & Klein R (2007). Efficient RANSAC for point-cloud shape detection. *Comput Graph Forum* 26(2), 214–226. <https://doi.org/10.1111/j.1467-8659.2007.01016.x> SMASH

- Shanbhag AG (1994). Utilization of information measure as a means of image thresholding. *CVGIP: Graph Models Image Process* 56(5), 414–419.
- Thiery C (2015). Tomographie à rayons X. Techniques d'analyse, in *Technique de l'Ingénieur*, France. <https://doi:10.51257/a-v3-p950> SMASH
- Turner TD, Gajjar P, Fragkopoulos IS & Roberts KJ (2020). Measuring the particle packing of l -glutamic acid crystals through X-ray computed tomography for understanding powder flow and consolidation behavior. *Cryst Growth Des* 20(7), 4252–4263.
- Vincent L & Soille P (1991). Watersheds in digital spaces: An efficient algorithm based on immersion simulations. *IEEE Trans Patt Anal Mach Intell* 13(6), 583–598. <https://doi.org/10.1109/34.87344> SMASH
- Wang XZ, Roberts KJ & Ma C (2008). Crystal growth measurement using 2D and 3D imaging and the perspectives for shape control. *Chem Eng Sci* 63(5), 1173–1184. <https://doi.org/10.1016/j.ces.2007.07.018> SMASH